

F30: CCD-Spectroscopy

Yajie Liang and Leon Tschesche

supervised by: Stephan Stock

on March 25th – 27th 2019

handed in as long report on: July 22, 2019

Abstract

This experiment has been performed as part of the advanced lab course for physics students (FP) at the University of Heidelberg.

The theoretical and experimental basics needed for the understanding of the conducted measurements and analysis is introduced and important concepts of the CCD are presented and discussed.

The characteristics of the CCD used in the KING telescope on the Königstuhl, Heidelberg, are analysed using data we recorded.

Additionally we will apply some basic data reduction techniques to our data and see the direct consequences of these.

Furthermore we used archival images from the Hubble Space Telescope (HST) to produce a color magnitude diagram (CMD) to estimate the distance, age, and metallicity of a cluster.

Finally if the weather allows it, we will make our own observation of a cluster and analyse it with such color magnitude diagram.

Contents

1 Fundamentals of astronomical observation	3
1.1 Basics of CCD detectors	3
1.1.1 Advantages of CCD detectors	3
1.1.2 Noise sources of CCD detectors	4
1.2 Basics of astronomical data	5
1.2.1 Data-influencing effects	5
1.2.2 Data reduction	5
1.3 Basics of photometry	6
1.3.1 Magnitudes	6
1.3.2 Observation of a star	7
1.4 Basics of spectroscopy	8
1.5 Relevant astronomy	8
1.5.1 Globular clusters	8
1.5.2 The Hertzsprung-Russel-Diagram	8
1.5.3 Color-Magnitude-Diagram	8
1.5.4 Analysis with a CMD	9
2 Layout and execution of the experiment	10
2.1 CCD and telescope	10
2.2 Execution of the measurements	10
2.3 Analysing archive data from BS90	11
3 Measurement and Evaluation	12
3.1 Characteristics of the CCD and data reduction	12
3.1.1 Bias correction	12
3.1.2 Dark measurements	12
3.1.3 Flat-field correction	13
3.1.4 Linearity and saturation area	14
3.1.5 Sensitivity and noise	15
3.2 CMD of globular cluster BS90	17
3.2.1 PSF fitting	17
3.2.2 Zeropoint calibration	17
3.2.3 Plot CMD and fit isochrones	18
4 Discussion	19
References	21

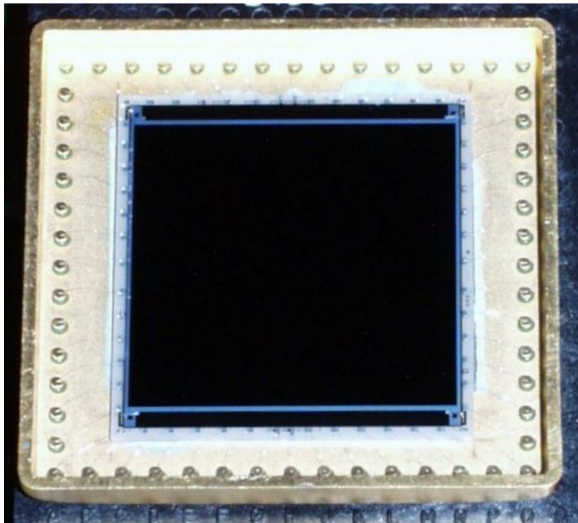
List of Figures

1	Examples taken from the Manual [6]	3
2	Example of the different diagrams	9
3	Pictures taken from KING and the dome where it is located	10
4	Dark current measurements at different Temperatures	12
5	Data of the dark current measurement plotted and fitted	13
6	Histograms of the normalized master flat-fields for the 3 filters of our CCD	14
7	Example of an image getting corrected with the master flat-field	14
8	Verifying the linearity in 2 filters and determining the saturation area	15
9	Region for Noise	15
10	Variance of the difference image versus the median counts of the images	16
11	Histogram of the noise on both filters, required to find stars	17
12	The post-processed PSF of the I filter	17
13	Best <i>isochrone</i> fits for the CMD created with our zero point calibration	18
14	CMDs with the age and metallicity of [8] for the <i>isochrones</i>	19

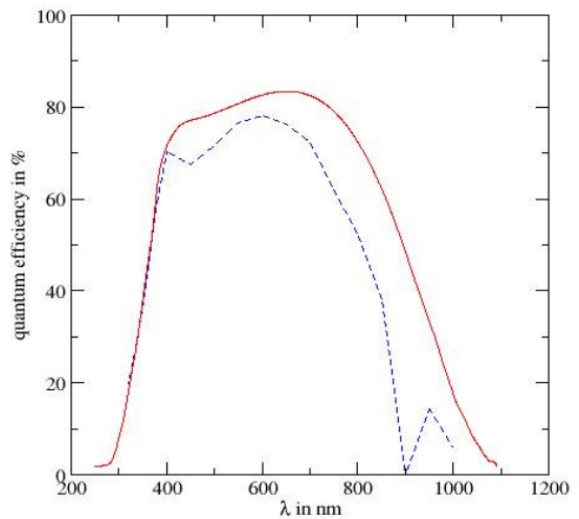
1 Fundamentals of astronomical observation

1.1 Basics of CCD detectors

Instead of photographic plates like in the beginning of photography, people now widely use *Charged coupled devices* (CCDs) for the detection of optical radiation, in visible light cameras and in modern telescopes. The working principle of CCD is as follows: Electrons produced by photoelectric effect are collected in the potential walls of the capacitors on a two-dimensional array of pixels made of semiconductors capacitors. The collected charges are first read out by being shifted column by column and sent to counting device (output register) at the end of each horizontal line, which consists of a series of electrodes. Then the signal is amplified and an offset, also called bias, is added so it can be digitalized by an *Analogue digital converter* (ADC). The offset is required to ensure all values are positive since the ADC can only handle values greater than zero. After calibrating and analysing numerical data one can reconstruct the distribution of observed astronomical objects.



(a) A CCD detector



(b) Quantum Efficiency

Figure 1: Examples taken from the Manual [6]

1.1.1 Advantages of CCD detectors

Some of the numerous perks the CCD offers, besides delivering the data in digital form, are:

- **Good spatial resolution:** The resolution and the field of an image taken by a CCD depend on its number of pixels. With large amount of pixels in small volume of CCDs one can see the details at the surface of the studied object.
- **Very high quantum efficiency over large spectral window:** CCDs are sensitive to the radiation in a large wavelength domain. The fraction of detected photons on CCD reaches more than 50% ($> 80\%$ at certain wavelengths), which enables the detection of very faint objects.
- **Very good linearity:** There exists good linear relation between measured signal and incoming photon flux, which is proportional to the exposure time, with a large saturation threshold and no requirement on minimum exposure time. CCDs are linear to an accuracy of about 0.1% within their dynamical range.

- **High photometric precision and a reliable rigidity:** Since CCDs are made of solid elements and the position of each pixel is fixed in a rigid way during the production, there's usually no physical distortion and the sensitivity of CCDs is stable in time.
- **High dynamic range:** The brightest object that can be detected depends on the capacity of pixels to collect photoelectrons before they saturate, which increases with the individual pixel. The faintest object that can be detected are determined by the signal to noise ratio. The dynamic range represents the maximum possible ratio between the fluxes of the faintest objects and the brightest ones, which is small for CCDs, so that people can detect objects with high difference in magnitudes at the same time.

In this experiment we will confirm the linearity of our CCD and analyse different noise sources.

1.1.2 Noise sources of CCD detectors

We will specifically look at three different noise sources when observing a flat illuminated surface:

- **Read-out Noise σ_r :** The read-out noise originates from the gate amplifier and doesn't scale with the number of incoming or detected photons. This error can be measured by looking at a difference image of two 0 milliseconds exposure time images [5] or measuring the scatter of the bias, which is what we will do. The bias will be recorded in each picture as a 26 pixel extension of our image at the right edge.
- **Photon Noise σ_{ph} :** Incoming Photons are subject to fluctuations which can be described with Poisson statistics, meaning the amount of measured Photons of a uniformly lit area can vary with $\sqrt{N_{ph}}$. Further we have to consider the quantum efficiency and the fact, that the final picture we can see is acquired through an ADC, which counts κ electrons as one *count*. This all leads to a formula for the photon noise as follows:

$$\sigma_{ph,d}^2 = \frac{\eta}{\kappa} N_{ph,d}. \quad (1)$$

Where $N_{ph,d}$ will be the median of the *counts* in the image.

- **Pixel response non uniformity Noise σ_{PRNU} :** Each pixel has a slightly varying quantum efficiency, resulting in a noise which scales directly with the incoming photon number. It scales linear with photon number compared to the square root dependency of σ_{ph} . The scaling factor is of the order 10^{-2} . Resulting from those dependencies we expect σ_{PRNU} to dominate for high signals and σ_{ph} for the lower ones. Since the pixel difference is a characteristic of each pixel, it generally should be the same for images taken with the same exposure time of the same objects.

If we now consider those noise sources we can write the total noise of the image as follows:

$$\sigma_{tot,d}^2 = \sigma_{PRNU,d}^2 + \sigma_{ph,d}^2 + \sigma_{r,d}^2. \quad (2)$$

As mentioned above we will be able to determine the read-out noise directly from the image by taking the standard deviation in the overscan region. But the other 2 noise sources are not as easily accessible since even with the approximation of $\eta = 1$ we still are missing our gain and we don't know the exact scaling factor for our *prnu* noise. For that we will utilize the characteristic of σ_{PRNU} being the same for observation of the same object with same exposure time. If we record two images in sequence and subtracts each pixel value we acquire the so-called *difference*

image. It will consist only of the other 2 noise sources, since we removed the initial signal as well as the σ_{PRNU} . We can express the scatter of that image as follows:

$$\sigma_{diff,d}^2 = 2(\sigma_{ph,d}^2 + \sigma_{r,d}^2) \quad (3)$$

From eq (3) and eq (2) we can now determine $\sigma_{ph,d}$ and σ_{PRNU} .

1.2 Basics of astronomical data

Besides the noise we looked at there are several other physical effects one has to take into consideration when analysing the image.

1.2.1 Data-influencing effects

Some effects influence data quality and there are different methods to deal with them:

- **Noise and dynamic range:** Despite of large dynamic range of CCDs it is not always possible to simultaneously assure a good signal to noise ratio for weak objects of interest, while not saturating very bright stars. Thus it is important to select exposure time carefully depending on the purpose of the observation.
- **Extrema of data:** A certain amount of pixels on the detector are "dead", i.e. produce no physically significant signal at all. The amount and distribution of these pixels stays the same over time. Additionally some other pixels are activated by cosmic rays such as electrons, γ -rays, muons, etc. Around the impact position the pixels are saturated or show high numbers of counts. The distribution of these pixels is random and the number of them depends on integration time. To get rid of these extrema people use method called *dithering* or *jittering* by taking several exposures (at least 5) with the telescope being moved slightly between each exposure. The multiple frames are then aligned and the median of each pixel of the combined image is determined. With this method the signal to noise ratio is also improved without saturating brighter sources.
- **Diffraction by aperture:** Light is diffracted when passing through apertures, the diffraction effects increase with decreasing aperture size. The degree of spreading (blurring) of a point object is a measure for the quality of an imaging systems, which is described with a *Point spread function* (PSF). For a diffraction-limited optical system operating in the absence of aberrations, i.e. a perfect lens with a uniformly illuminated circular aperture, the PSF is the Airy disc, a bright central region surrounded by concentric rings. In astronomy the Airy disc is used to determine the quality and alignment of the optical components of a telescope. The Rayleigh criterion for barely resolving two objects is that the centre of the Airy disc for the first object occurs at the first minimum of the Airy disc of the second.

1.2.2 Data reduction

The previously described effects and corresponding methods don't include any alteration of the taken data. Other effects can be treated right away without consideration of the observed objects. Those effects can be negated through altering the data in certain ways. The ones which we will take a closer look in this experiment are:

- **Bias:** The previously mentioned offset, the bias, added to prevent malfunctioning of the ADC has to be determined and subtracted. As also mentioned above we will determine it from a small border region in our images called the *overscan region*. The bias will be determined for each picture separately and subtracted.

- **Dark current:** Dark current refers to the signal produced through the thermal energy of the electrons in the CCD. It leads to a detected signal even if no photons are reaching the CCD. It depends on the temperature as follows:

$$I_{dark} = \text{const } T^{\frac{3}{2}} e^{-\frac{E_g}{k_b T}}. \quad (4)$$

E_g is the bandgap of the material in the detector, which is silicone in our case, T is the temperature and k_b is the Boltzmann constant. We will measure the temperature dependency of the dark current by taking images with the shutter closed, i.e. no photons will be detected, while the CCD is getting cooled down. Since the measured *counts* are proportional to the current measured, which with no detectable photons is only the dark current, we can verify the eq (4) as well as determine the bandgap of silicone. If the dark current value is not negligible at the working temperature, one would have to subtract it from every image as well.

- **Flat fields:** Different sensitivity of each pixels due to imperfect production of the CCD results in small scale variations. On the other hand, there exists large scale variations caused by the optics (*vignetting*) and contaminations in the optical path. These variations, causing difficulties in comparing objects from different region, are however constant at least during the observation. For corrections one exposes the whole detector to a structureless and homogeneously emitting surface, i.e. flat field, and records the variations. In practice the flat field is provided either by a white surface hanging on the inner side of the dome or the twilight sky. Though the twilight period is rather short, the sky-flatfield provides the same condition as real observation and is thus preferred. For the data reduction purpose one has to take multiple images and take median value for each pixel to create a master flat-field. Then you normalize the master flat-field with its median to produce a *relative image matrix* which contains the relative strength of each pixel to each other. Every measurement frame is then later divided by that normalized master frame. Each filter requires its own master frame since the optical set up is changed.

1.3 Basics of photometry

With CCD detectors one can measure the radiation flux or intensity of an astronomical object reaching the earth. This process, photometry, uses the unit of magnitudes and is essential to understanding stars and other astronomical subjects.

1.3.1 Magnitudes

The luminosity of a star L is defined as emitted energy per unit time. The flux reaching an observer in a distance d is given by $F = \frac{L}{4\pi d^2}$. The intensity is defined as flux per solid angle. One can differentiate between several different magnitudes:

- **Instrumental magnitude:** For measurements by the same instruments and under similar conditions, the comparison of different sources is realised by instrumental magnitudes. The measured counts are converted to a logarithmic scale with arbitrary zero point:

$$m_{instr.} = zeropoint - 2.5 \log_{10} (\text{counts}) \quad (5)$$

The counts is calculated either by simply summing over an aperture centered on the star, i.e. aperture photometry, or by fitting a PSF to the profile of the star, i.e. PSF photometry.

- **Apparent magnitude:** The brightness of stars perceived from earth, the apparent magnitude, was once classified by eye ranging from 1 for the brightest stars to 6 for barely visible stars. It was later quantified assuming a logarithmic perception. For the flux of two stars it means:

$$\frac{F_2}{F_1} = 100^{(m_1 - m_2)/5} \quad (6)$$

With the help of standard stars the difference between instrumental magnitude and apparent magnitude is determined and observed magnitude is then calibrated. The effects of different instruments and circumstances for comparison of magnitudes are hence eliminated.

- **Absolute magnitude:** To compare objects in different distance one can use the absolute magnitude, which is the apparent magnitude M of an object if it were in distance of 10 pc from our sun. The relation between apparent and absolute magnitude satisfies

$$\frac{F_{in10pc}}{F} = \left(\frac{d}{10pc}\right)^2 = 100^{(m - M)/5} \quad (7)$$

with d as the distance between the star and the observer in pc. However d is usually unknown which makes it hard to compare stars absolute magnitude. One could calculate the distance of an object with absolute and apparent magnitude as follows

$$d = 10^{\frac{m - M + 5}{5}}. \quad (8)$$

The expression $m - M$ is called the distance modulus.

From the absolute magnitude of a star at the same distance as a reference star with known luminosity and absolute magnitude, it's possible to determine its luminosity:

$$\frac{F_2}{F_1} = \frac{L_2}{L_1} = 100^{(M_1 - M_2)/5} \quad (9)$$

- **Bolometric magnitude:** The Bolometric magnitudes M_{bol} corresponds to the flux integrated over all wavelengths. Its direct measurements are only possible by space observatories. From earthbound observations people have only theoretical estimate because of detector limitations and atmosphere's absorption of certain wavelength. Alternatively a wavelength dependent magnitude M_γ for luminosity in a certain wavelength range is used.

1.3.2 Observation of a star

Through observation people want to learn physical properties of a star. The flux is related to star's surface temperature, given by Stefan-Boltzmann law: $F = \sigma T_{eff}^4$ with $\sigma = 5.67 \times 10^{-8} \text{ W m}^{-2} \text{ K}^{-4}$ Stefan-Boltzmann constant and T_{eff} being the temperature of a black body emitting the same radiation power. Furthermore people are also interested in the mass of a star and its metallicity, from which its evolution can be deduced. In astronomy all the elements besides H, He and their isotopes are called metals which for a star is referred to as its metallicity. It is however not trivial to calculate the mass of a star from easily accessible observables.

1.4 Basics of spectroscopy

Spectroscopy is the measurement of the spectral intensity of the emitted light with high accuracy. But since the CCD image doesn't contain any direct information about color we use filters to extract those information out of multiple images.

Filters that transmit a certain part of the spectrum are used to obtain rough spectral information. A common used filter system is Johnson filter system with broad band filters, which contain U(ultraviolet), B(blue), V(visual, i.e. green), R(red) and I(infrared) filters.

To quantify spectral properties color index is defined as difference between magnitudes with different filters:

$$m_B - m_V = M_B - M_V = B - V. \quad (10)$$

The special characteristic of this color index is the invariance of the number. It is the same for apparent magnitude and absolute magnitude. It further gives information about the temperature of the star since the index gives us information about the spectrum of the star which we can connect to a temperature by looking at black body radiation spectrum. We will call the apparent magnitude of a certain Johnson filter with the letter given above.

To compare measurements with different filter systems a calibration with standard stars is applied. Assuming the transmission curve for the B filter is slightly different, the calibration of the instrumental magnitude can be calculated in a first order approach.

1.5 Relevant astronomy

With the magnitudes of those stars and corresponding color index we can now relate those to each other to find out more. But first we will introduce globular clusters.

1.5.1 Globular clusters

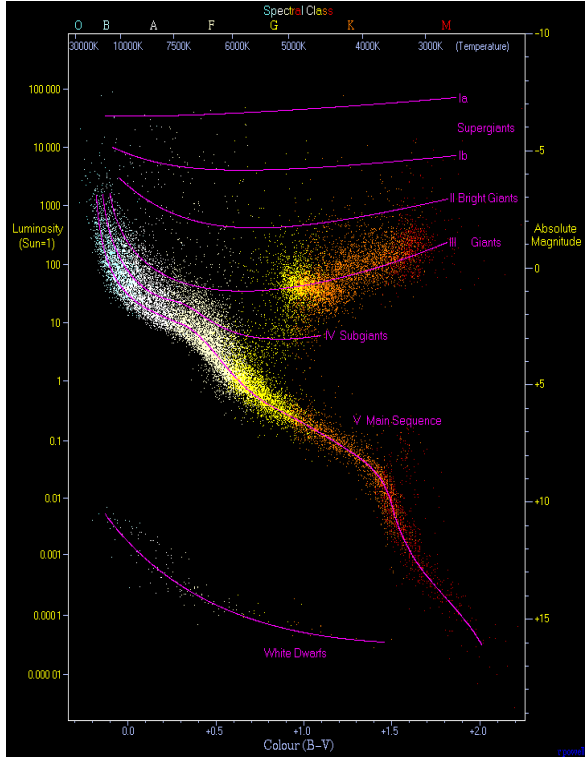
Globular clusters, spherically collection of stars, are by now counted to the oldest objects found in the universe. The stars in a globular clusters in our milky way are very metal poor, which indicates their formation in early stage of the universe when the interstellar matter was not enriched with heavier elements than hydrogen and helium. With about 150 globular clusters known, the distribution, velocity and composition of globular clusters provide information about the evolution of our galaxy. The age identification of globular cluster shows however large errors and discrepancies with different measurements.

1.5.2 The Hertzsprung-Russel-Diagram

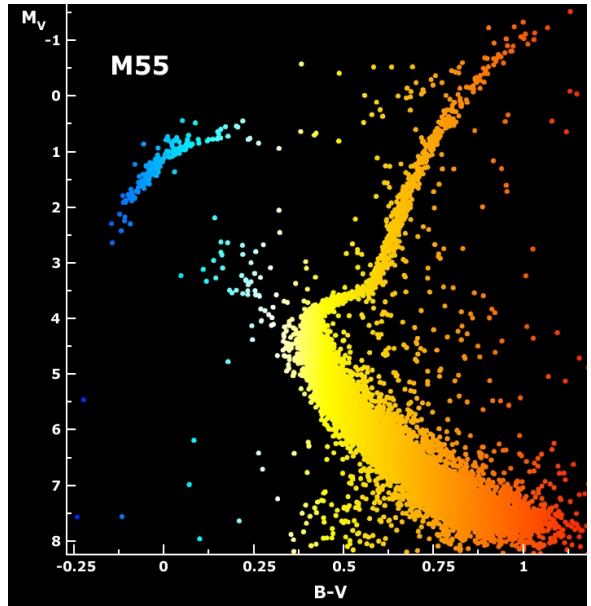
At the beginning of last century, Hertzsprung and Russel used data of photometrically measured stars, independently discovered the correlation between the spectral type, effective temperature and luminosity, as shown in Hertzsprung-Russel-Diagram (HRD). An example is of an HRD is shown in figure 2a. The majority of the visible stars experiencing the phase of hydrogen burning locate in the *main sequence* diagonal region. Different regions in the diagram indicate different masses, distances, evolution phases of stars. For example, O stars refers to young, massive and luminous objects.

1.5.3 Color-Magnitude-Diagram

In practice it is often difficult to produce a HRD, instead a Color-Magnitude-Diagram (CMD) plotted with the apparent magnitude against a related color index, determined directly from



(a) Hertzsprung-Russel Diagramm [7]



(b) Color-magnitude Diagram [3]

Figure 2: Example of the different diagrams

observations with two filters, is used. A CMD provides also large amounts of important information as a HRD. Globular Clusters are well suited for the analysis with a CMD, since all their stars are located at the approximate same distance and have the same metallicity. This leads to an easy approximation of the distance modulus. The CMD of a globular cluster has a characteristic form as seen in figure 2b.

1.5.4 Analysis with a CMD

Assuming all stars within the cluster have similar ages, one can read off the age of the cluster from the CMD. Since massive and luminous at the top left end of the CMD burnt their hydrogen in their cores within short lifetime and turned into a red giant, the older a cluster is, the lower mass stars move from main sequence into the red giant branch. The shifts to stars with lower mass and luminosities, i.e. turn off point, whose position depends also on metallicity of the cluster, are good indicators for age of older clusters. For young clusters there may exist ambiguity.

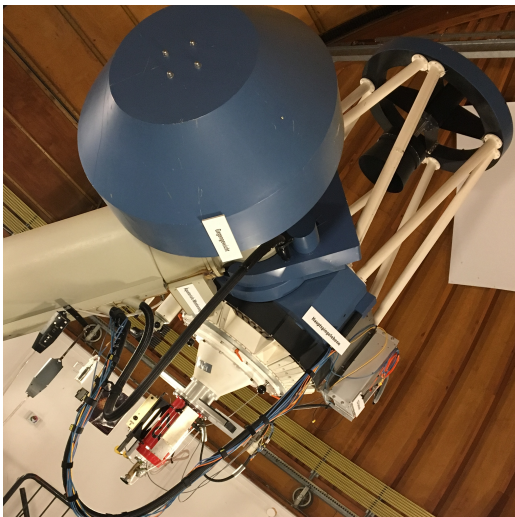
Since in a globular clusters one can approximate, that the stars are at the same distance with same chemical composition as well as similar ages one can read the distance to cluster from a CMD. The position of the main sequence is compared to the position of a cluster with known distance. With some presumptions ignoring effects of different metallicities and of attenuation by interstellar dust, the distance modulus of the cluster can be deduced by the shifts. Alternatively it can be compared to predictions of its position by theoretical models, for example *isochrones*, i.e. curve representing stars of the same age.

2 Layout and execution of the experiment

As mentioned above we will analyse the different characteristic of our CCD, do some of the basic data reduction and determine the bandgap of silicone. Afterwards we will create a CMD from archive pictures of a globular cluster and fit an *isochrones* to determine its age metallicity as well as the distance modulus. The suggested schedule from [6] intends for us to make an observation ourself, process and analyse it. But since the weather was not fitting in the 3 days we booked the experiment, we didn't get to make said observation.

2.1 CCD and telescope

We use the **KING** (Königsstuhl Instrument of night-sky gazing) telescope located at the MPIA, Heidelberg, shown in figure 3a. Its main mirror is 70 cm diameter and focuses parallel light into the CCD detector, which is a *Loral/Lesser n2k2eb BI* thinned and back illuminated CCD. It has 2048 x 2048 pixel with a size of 3 cm x 3 cm resulting 15 μm per pixel and a quantum efficiency of up to 90%. We will operate it with 4 pixel counting as 1 since we aren't interested in the high resolution in this experiment. The filters, the shutter and the CDD detectors itself will be controlled from a UNIX computer via terminal. The flat surface needed will be provided by a white sheet hanging on the wall of the dome as shown in figure 3b.



(a) KING with CCD in the red box



(b) Flat surface for flat-field

Figure 3: Pictures taken from KING and the dome where it is located

2.2 Execution of the measurements

Firstly we need to cool the CCD detector. For that purpose, we evacuate the vessel containing the chip to around 10^{-6} mBar and fill it with liquid nitrogen. Before starting the cooling process we make ourselves familiar with the process of taking an image and write a macro to take images for us with constant exposure time in equidistant points in time, to observe the cooling process and the dark current. For that measurement it doesn't matter which filter is in use, since we have the shutter closed. Upon reaching our working temperature we make measurements of the

flat surface for all 3 filters, as well taking images with increase exposure time in the R filter to check the linearity as well as the saturation area of our the CCD. Afterwards we take pair images with increasing exposure time in the I filter for noise analysis as discussed in section 1.1.2.

2.3 Analysing archive data from BS90

In the second part we analyse archive pictures from the globular cluster BS90. They were taken July 13th - 18th 2004 from the Hubble Space Telescope (HST) with the filters F555W (V) and F814W (I) [1]. For that matter we will firstly determine the counts of bright stars in the image which are also in the star catalogue in *SIMBAD*. Then with apparent magnitude from the catalogue and the counts from our pictures we can determine the zeropoints for each picture, i.e. filter.

Since detecting all stars manually takes way too long, we use the program *STARFINDER*. We first analyse the Noise of the each picture, since the program takes the noise into account for the threshold what it registers as a star. Afterwards we create a PSF by showing the program roughly 10 *example stars*. After limiting the size of the PSF to 50 pixel and normalizing it we start the iterative process of star finding where it scans the whole picture to find objects similar to that of the PSF, where we set a lower bound threshold relative to the noise. After doing that for both pictures individually we use a python script to match found stars from both lists by using a max deviation of 1 pixel. This matched star list now contains stars where apparent magnitude of both filters are known. Afterwards we can plot a CMD from that and fit an *isochrone* to it to determine age, metalicity and distance of BS90.

3 Measurement and Evaluation

3.1 Characteristics of the CCD and data reduction

We visualize and analysis the data image using *Python* with the packages *astropy*, *ccdproc*, *numpy* and *matplotlib* and the image display program *ds9* to check the .fits images produced by the CCD detector and the *python scripts*.

3.1.1 Bias correction

As explained in section 1.2.2, we first determine the bias from the overscan region on the right edge of CCD images of dark measurements. We then subtract said bias from the whole image to get a bias free image. We determine the overscan region to be in the are $x > 1024$ for all y with *ds9*. In figure 4 you can see 3 different measurements with shutter closed and bias subtracted. We can clearly see the overscan region as long as you have a signal. The bias of the uncorrected first image in figure 4a is 1374.0 ± 5.2 , of the second image in figure 4b 1334.0 ± 1.8 and of the last image in figure 4c 1350.0 ± 1.7 .

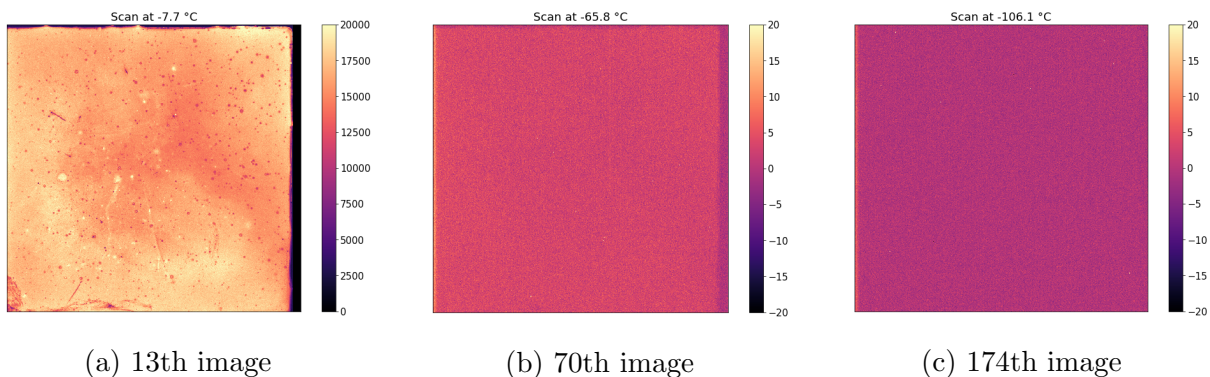


Figure 4: Dark current measurements at different Temperatures

3.1.2 Dark measurements

From the bias subtracted pictures we can now extract the dark current by calculating the median of each picture. By plotting $\text{counts}T^{-\frac{3}{2}}$ over T^{-1} on a log scale seen in figure 5 we can determine the band gap by fitting an equation to the data set. To get the fit function we rearrange eq (4) to match the quantities we have plotted. This gives a function as follows:

$$\text{counts } T^{-\frac{3}{2}} = \text{const } e^{-\frac{E_g}{2k_B T}} \quad (11)$$

where Boltzmann constant $k_B = 8.617 \cdot 10^{-5} \frac{\text{eV}}{\text{K}}$ and E_g is the band gap of silicone. We now fit a function on that data set and determine E_g from on the 2 parameters. We fit with 3 different fit ranges, indicated by the different coloured dotted lines to approximate an error with those fits. We do this since the approximation seems to deviate a lot for lower temperatures, but still results in a small error in the range 2 - 3 meV. This can be explained by remembering that this is a log scale, meaning the values on the bottom right of the fit are several magnitudes smaller than the values that seem to be right on the fit in the top left. Hence we use the fit range variation to approximate an error for our measurement which leads us to a value of $E_g = 1.19 \pm 0.4 \text{ eV}$. The literature value is given as 1.15 eV. This 1σ deviation as well as the overall deviation of the fit for lower temperatures can be explained by two main reasons.

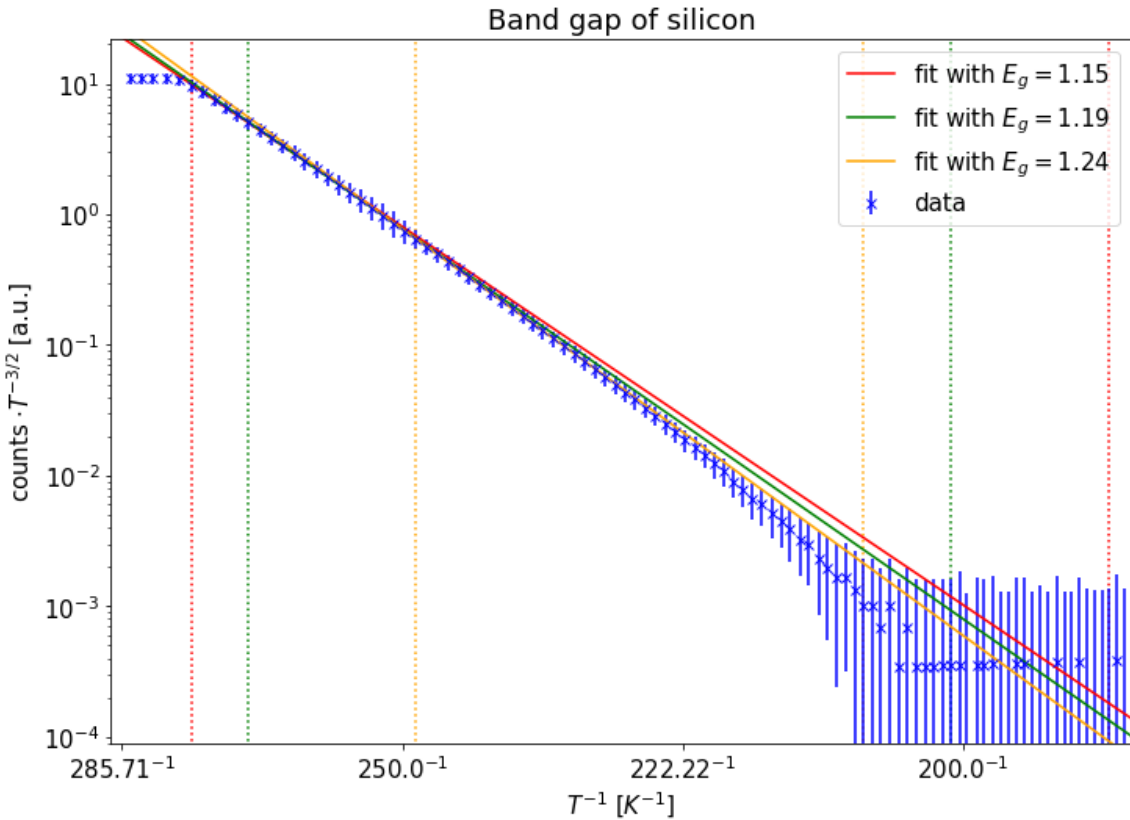


Figure 5: Data of the dark current measurement plotted and fitted

First, the temperature is only measured once at the start of the exposure time, with no further information saved about the change over the exposure time. Also the temperature has no error associated with it since we didn't average over several measurements nor did we have any information on the precision of the sensor.

Second, the band gap is not constant for different Temperature. It has a dependency on T which can be described [9] as follows:

$$E_g = E_{g,0} - \frac{\alpha T^2}{T + \beta} \quad (12)$$

α and β are material constants, T is the temperature and $E_{g,0}$ is the band gap at 0 K.

The second argument leads to a higher band gap for lower temperature, which is reflected in our data as well since the fit with the higher band gap is the ones which is more fitting for the lower temperatures.

Looking at the image in figure 4c we can conclude, that at our working temperature of roughly -106°C the dark current is indeed small enough to ignore.

3.1.3 Flat-field correction

After subtracting the bias from the individual flat-field images, we combine the individual flat-field images to a single image (the master flat-field). We set all values below a certain threshold to 0 so those pixel get valued as NAN when evaluating images. Then we normalize the master flat-field by dividing it by its median and create a histogram for this master flat-field as shown in figure 6.

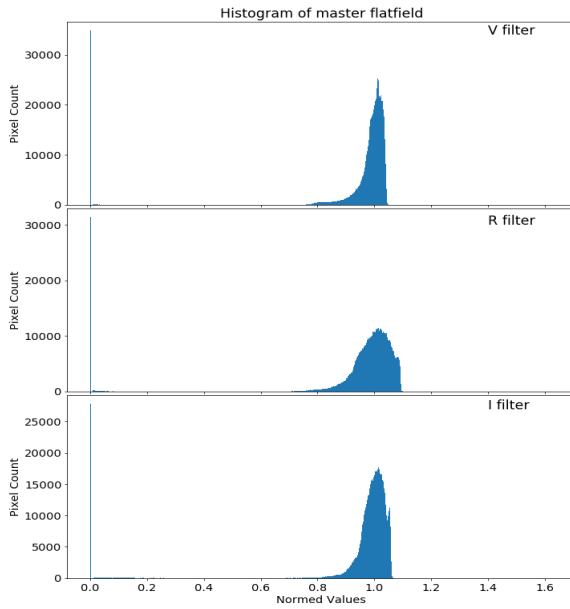


Figure 6: Histograms of the normalized master flat-fields for the 3 filters of our CCD

son of two plots is shown in figure 7. One can see the symmetrical effects very clearly in 7a as well as the optical containments. After the correction seen in figure 7b we can see that the image has become *flat*, i.e. evenly distributed, by changing its range from 6000 pixels to less than 350 pixels. The green area here shows NAN values, meaning we tried to divide by a zero of the master flat-field. The difference between the pixels can be attributed to the noise we discussed in section 1.1.2. Though statistical noise seems to be not the only source since one can see some weird shape in the image which seems to be not statistical nature.

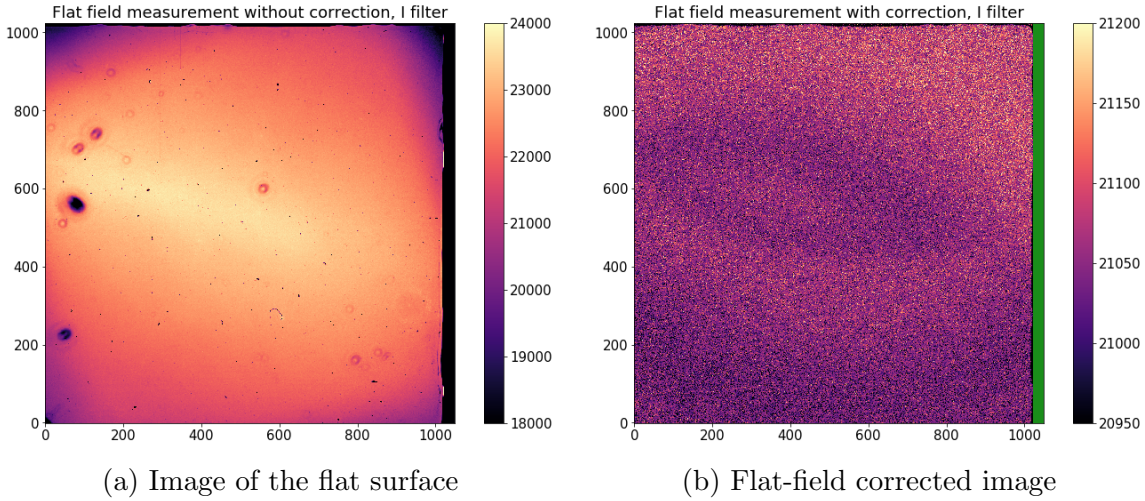


Figure 7: Example of an image getting corrected with the master flat-field

3.1.4 Linearity and saturation area

To verify the linearity as well as the saturation value of the chip, we plot the signal of each flat-field-corrected image against its exposure time. We do this for two different filters, I and

The bar at 0 indicates the overscan region (which has 26624 pixels) as well as dead pixels or dead regions on filter through contaminations. Most of pixel group around the median value, i.e. 1 on the x-axis, though there are a lot more below 1 than above. This can be explained by realizing that the group below one has a lot more sources than only the optical effects like *vignette* effect which are the reason for the deviation above as well as under. The group under 1 contains all the optical containments from which not all result in a full photon block, rather they only reduce the photon amount.

To grasp what those effects could look like and how we compensate those, we perform a flat-field correction for a single flat-field image with the I filter and compare the uncorrected image with the corrected one. The compari-

son of two plots is shown in figure 7. One can see the symmetrical effects very clearly in 7a as well as the optical containments. After the correction seen in figure 7b we can see that the image has become *flat*, i.e. evenly distributed, by changing its range from 6000 pixels to less than 350 pixels. The green area here shows NAN values, meaning we tried to divide by a zero of the master flat-field. The difference between the pixels can be attributed to the noise we discussed in section 1.1.2. Though statistical noise seems to be not the only source since one can see some weird shape in the image which seems to be not statistical nature.

R , where we just take one image of the pairs taken with the I filter. To determine the deviation from a perfect linear relationship we calculated R^2 , which is closer 1 the better the linear dependence is, its exact formula can be found at [4]. We calculate it for both linear fits and determine the saturation area with data from both measurements. The data and fits are shown in figure 8.

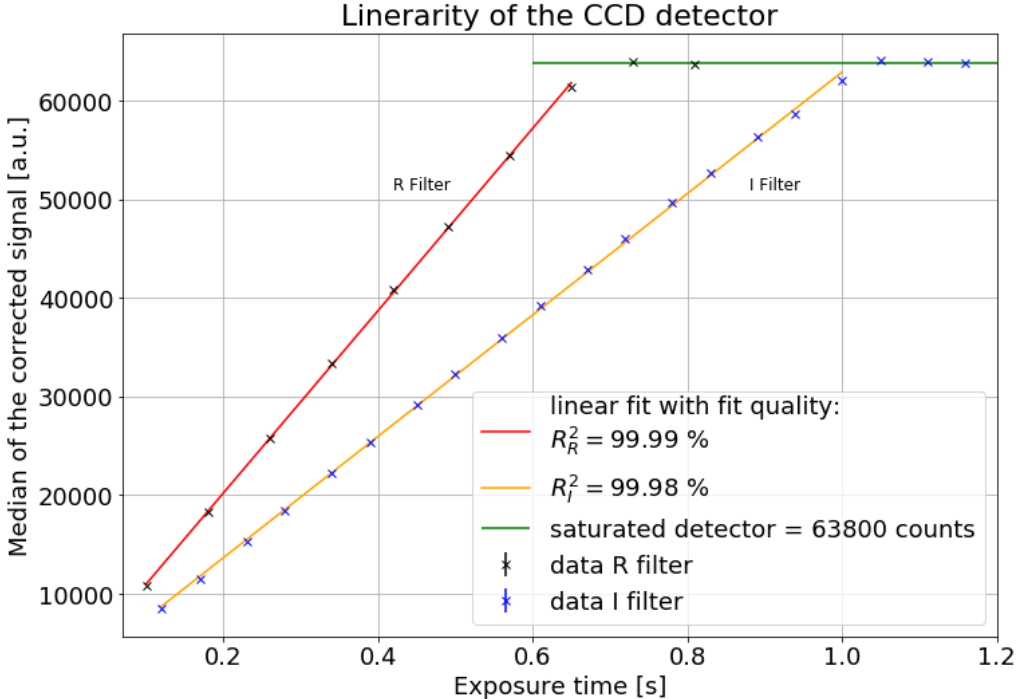


Figure 8: Verifying the linearity in 2 filters and determining the saturation area

Both filters show an exceptionally good R^2 , deviating less than 0.02% from the linear approximation. The saturated area can get determined to around 63800, meaning we should not exceed the 60000 counts if we wish to guarantee the linear characteristic from the CCD detector. Lastly we also see the dynamical range of the detector, since the filters take saturated at different exposure times which is a consequence of the spectrum of our light source (in our case the lamp illuminating our flat surface).

3.1.5 Sensitivity and noise

To analyse the noise and calculate the gain with it we first chose an image pair with around 30000 counts and select a region around the middle which is as uniform as possible. That region is pictured in figure 9. First off we can calculate the read-out noise $\sigma_{r,d}$ by calculating the scatter in the overscan region. Second we calculate the total noise $\sigma_{tot,d}$ in that chosen area. We then continue to calculate the difference image of the chosen image pair and calculate the $\sigma_{diff,d}$ in the chosen region. We can then use eq (3) and (2) to calculate $\sigma_{ph,d}$ and $\sigma_{prnu,d}$ shown in table 1.

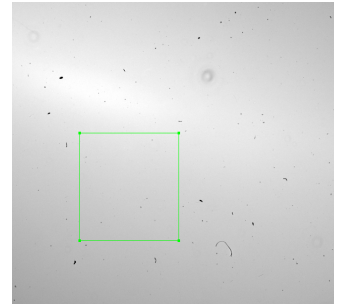


Figure 9: Region for Noise

As expected the σ_{prnu} dominates for high signal sources and the read-out noise is really small compared to the other noises caused by the independence on N_{ph} .

$\sigma_{tot,d}$	$\sigma_{diff,d}$	$\sigma_{rt,d}$	$\sigma_{ph,d}$	$\sigma_{prnu,d}$
264.3	75.9	2.1	53.6	258.8

Table 1: Summary of the errors for an image with 30000 counts

We can now calculate the gain from $\sigma_{ph,d}$ by using eq 1 and approximating η to be one. The gain gets calculated to $\kappa_1 = 10.85 \pm 0.03$ which is double the value we expected considering the *header* of our fits say that the gain is 5.

We can also calculate the gain differently. By inserting eq 1 into eq 3 directly without calculating $\sigma_{ph,d}$, we get a linear dependency of $\sigma_{diff,d}^2$ on $N_{ph,d}$. If we now calculate the difference image of pairs with increasing median counts, i.e. increasing exposure time, we can plot the variance of these difference images versus the average of the median counts in the pair. This is shown in figure 10.

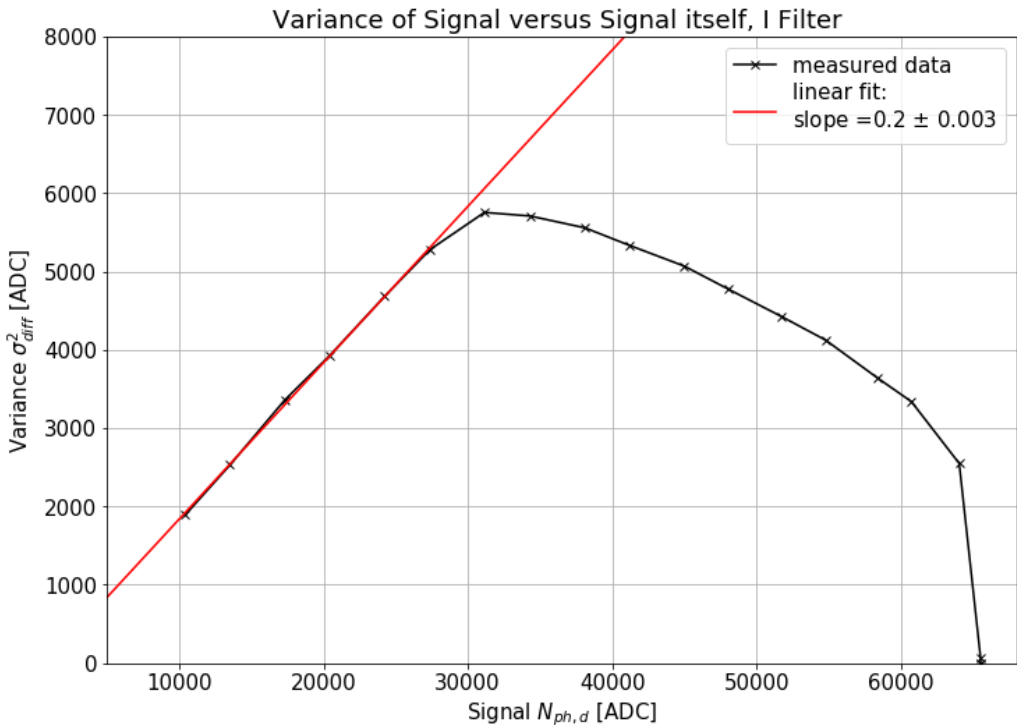


Figure 10: Variance of the difference image versus the median counts of the images

We can see that the linear dependency is very good till around 30000 counts, where it seems like other effects start to dominate which we didn't consider beforehand. Hence we will do the linear fit only till roughly 30000 counts to ensure the correctness of the fit. With that and the assumption of η being one we can relate the slope to κ by the double of its inverse $2slope^{-1}$. This leads us to a gain of $kappa_2 = 10.02 \pm 0.13$. As already mentioned this is still double the value we expected, but this time it is exactly double the value.

3.2 CMD of globular cluster BS90

We do most of the analysis for this part on a computer provided by the MPIA, which has *STARFINDER* already installed as well as *ds9* to view the pictures from the HST.

3.2.1 PSF fitting

To perform the PSF scan we first need *STARFINDER* to determine the noise of both pictures. The noise histograms are shown in figure 11. The dotted line is a Gaussian distribution fitted to the histogram to determine variance.

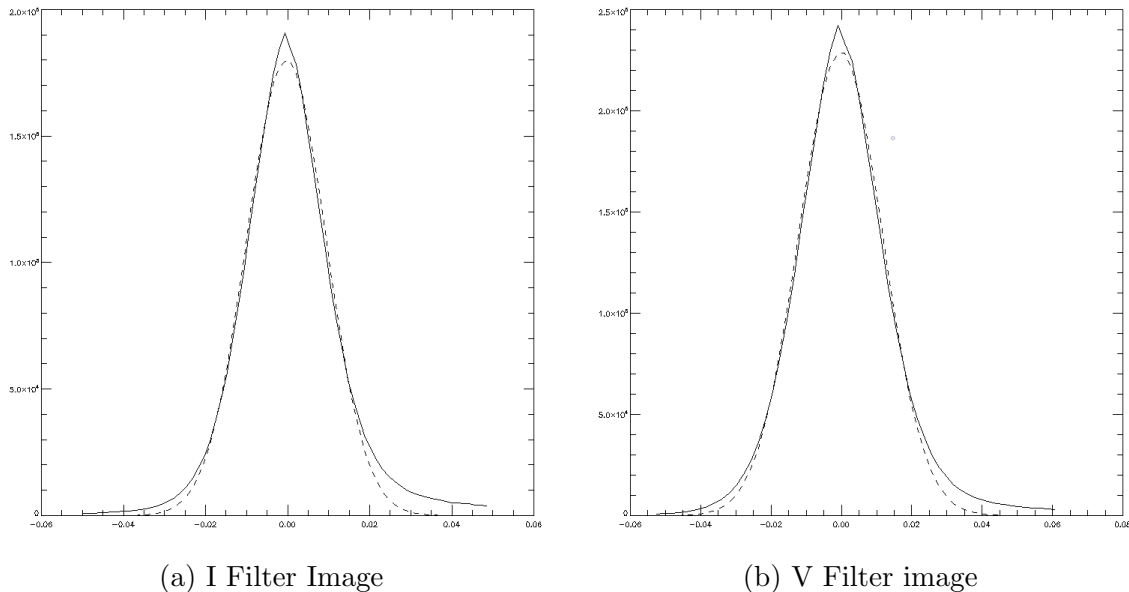


Figure 11: Histogram of the noise on both filters, required to find stars

After determining the noise we need to create a PSF so the program can search for the stars. We select 14 isolated, unsaturated stars. On a bounding box around the stars, an average PSF for the entire image is first created. Per editing we improve and optimize the PSF by limiting its pixel range and normalizing it, as seen in figure 12.

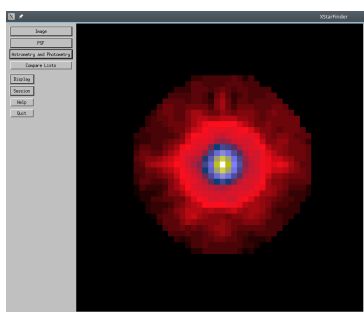


Figure 12: The post-processed PSF of the I filter

Now we let the program determine all possible stars. All sources above a certain threshold above the background level are detected as potential stars. All potential stars are then fitted with the PSF and the results of this fitting is subtracted from the science image. This step is performed iteratively. That way we can disentangle and correctly account for the flux of overlapping sources.

3.2.2 Zeropoint calibration

Since the measurements were carried out with two filters a calibration is needed in order to compare their results. We overplot the HST images with data base *SIMBAD*. We select 12 reference stars, which were calibrated themselves from true standard stars, write down the V and I magnitudes and measure their counts in both Hubble images. The instrumental magnitude is compared with the CATALOG objects to calculate the individual zero points for all objects for

both filters according to formula:

$$zeropoint = m_{CATALOG} + 2.5 \log_{10} (counts) \quad (13)$$

We take the median as final zero point values, which gives us $zero_V = 25.15702$ and $zero_I = 25.14337$. The apparent magnitude of found stars by PSF fitting can then be calculated by eq 5 with the calibrated zero points. We then use the mentioned python script provided by our tutor, to match all stars as well as write down their apparent magnitudes V and I which get calculated with the zero points we updated in the python script.

3.2.3 Plot CMD and fit isochrones

We plot V versus V-I of these stars and thus obtain the CMD of BS90. Then we plot a set of theoretical *isochrones* in the CMD, using another given Python script in which we can change the fit parameters, i.e. age, metallicity and the shift, i.e. the distance modulus, in the V axis, which gives us the distance to the cluster. Our best fit is shown in figure ??.

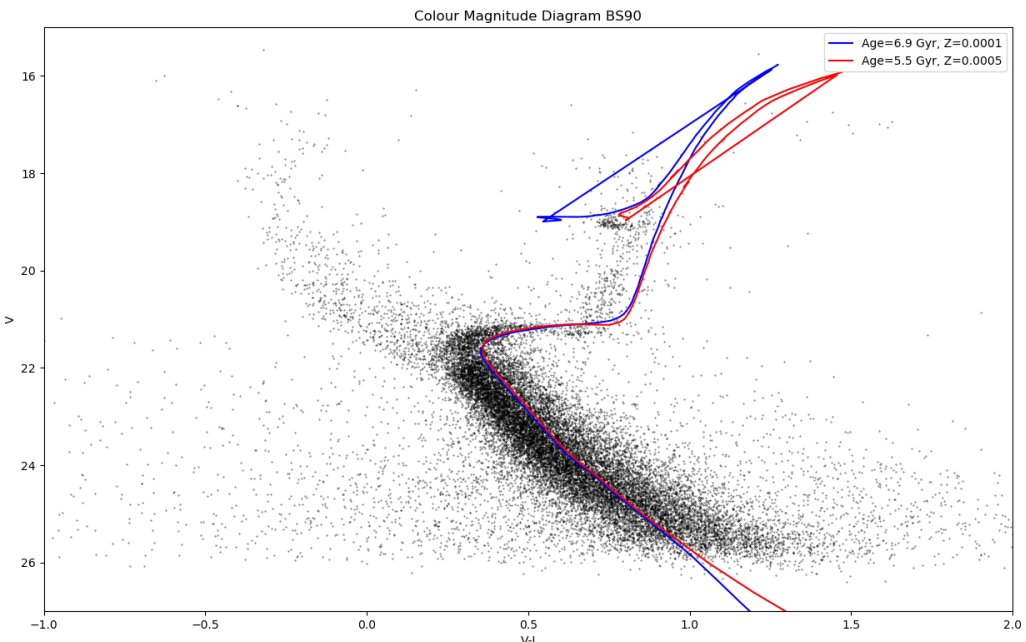


Figure 13: Best *isochrone* fits for the CMD created with our zero point calibration

We used a shift of 18.8 mag for these *isochrones*, which would correspond to 57.5 kpc distance to BS90. The parameter for the *isochrones* we fitted is age = 6.9 Gyr with metallicity $z = 0.01\%$ and 5.5 Gyr with $z = 0.05\%$. While the turn off point and the main sequence fit quite nice for the *isochrones* in our CMD, the red giant branch doesn't fit very well to our CMD, pointing towards a fault in the analysis.

After researching for a while we found a paper [8] which used the same images to analyse the globular cluster BS90 and after comparing our values to theirs we noticed a big discrepancy in age and metallicity. While their distance modulus was almost the same as ours with 18.85 mag, 58.9 kpc, they approximated the age = 4.5 ± 0.5 Gyr and metallicity $z = 0.4 \pm 0.1\%$. We then fit the values from the paper to our CMD shown in figure 14a. We needed to change the shift to 18.3 mag to remotely get close to a good fit, which translates to a distance of 45.7 kpc. Nonetheless it is an even worse fit than what we had beforehand.

Then we researched the origin date of the images which we found from [1]. We then continued to determine the zeropoints calculated for the HST via the ASC zeropoint calculator [2]. From there we were able to determine the zeropoint for the filters to $zero_V = 25.733$ and $zero_I = 25.529$. With those new zeropoints we calculated a new cross match and plotted the CMD again, shown in figure 14b and this time the values of the paper fit really well for a shift of 19.0 mag, which translates to a distance of 63.1 kpc.

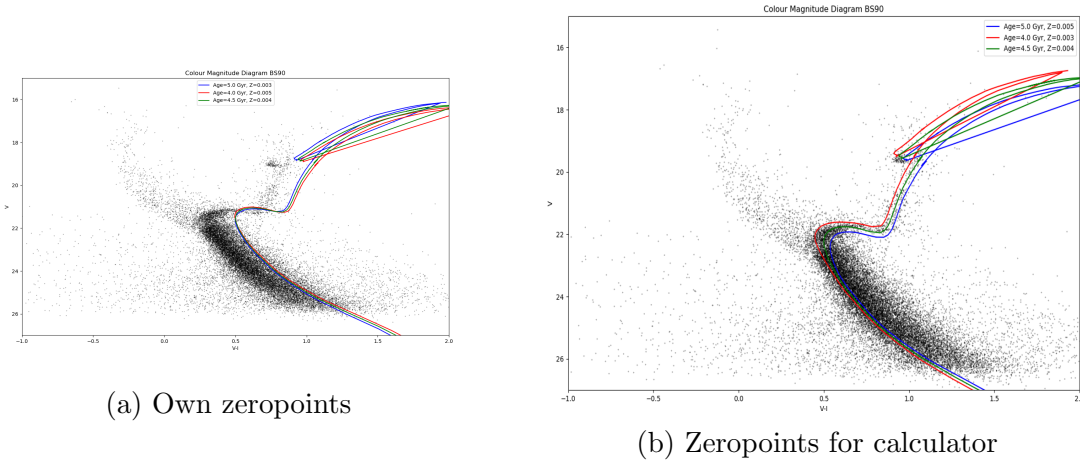


Figure 14: CMDs with the age and metallicity of [8] for the *isochrones*

4 Discussion

We were able to verify the linearity up to a very high accuracy and observe the dynamical range of the CCD. We learned about some basic data reduction techniques, such as bias subtraction and flat-field correction. We observed the dark current and looked at its temperature dependency. We concluded the cooling process is detrimental in reducing the dark current, which is otherwise a natural lower bound of the dynamical range and is deteriorating the sensitivity of the system by its stochastic nature.

The band gap determination has many errors sources which we didn't take into account, like the measurement of the temperature being not that accurate as well as the temperature dependency of the band gap. The decision to estimate an error by varying fit ranges made us overestimate the error given by the fit process by a factor of 10 (3 meV \pm 40 meV). But considering the obvious deviation in the lower energies one could pose the question why we didn't consider the energy dependency from the band gap to get a more accurate plot. But if we try to fit with α and β as parameter, it would become a very bad fit cause the parameters would correlated too much.

As already mentioned several times, the initial intention was to make an observation with the KING telescope of a globular cluster. If the weather would have been fitting, we would have used the data reduction we now just applied exemplary on some flat surface area. Afterwards analysing the images with the techniques performed on the archive pictures would have resulted in a CMD from our measurement, which would have been a nice way to finish this lab course.

To compare our results we read the reference paper [8]. As stated in the paper, the data are collected within the HST Program GO-10248, observed using the Wide-Field Channel (WFC) of ACS, centered on the association NGC 346, in the broad-band filters F555W(V-filter) and F814W (I-filter). With those information we were able to extract the zeropoints from the ACS zeropoint calculator [**HST zeropoints**] provided by Space Telescope Science Institute

and compare those zeropoints to the ones we calculated. The deviation can be explained by us not counting all photons in the pictures for a standard star or in general an inconsistent way of approximating the areas of the photons of a star.

References

- [1] URL: <http://www.stsci.edu/cgi-bin/get-visit-status?id=10248&markupFormat=html&observatory=HST> (visited on 03/27/2019).
- [2] URL: <https://acszeropoints.stsci.edu/> (visited on 03/27/2019).
- [3] J. Kaluzny (CAMK) B.J. Mochejska. *Globular cluster M55*. Astronomy Picture of the Day. NASA. Feb. 23, 2001. URL: <https://apod.nasa.gov/apod/ap010223.html>.
- [4] *Coefficient of determination*. URL: https://en.wikipedia.org/wiki/Coefficient_of_determination (visited on 07/15/2019).
- [5] Chris McFee. *Noise sources in a CCD. Readout noise*. 2019. URL: http://www.mssl.ucl.ac.uk/www_detector/ccdgroup/optheory/darkcurrent.html#Readout%20noise (visited on 07/10/2019).
- [6] Jörg-Uwe Pott. *FP30 - CCD photometry in modern astronomy*. 4.0.3. was used for most of this reports content. MPI for Astronomy. Aug. 10, 2017.
- [7] Richard Powell. *The Hertzsprung Russell Diagramm*. 2011. URL: https://en.wikipedia.org/wiki/Hertzsprung%20%93Russell_diagram#/media/File:HRDiagram.png.
- [8] Boyke Rochau et al. “The star-forming region NGC 346 in the small magellanic cloud with hubble space telescope accs observations. II. Photometric study of the intermediate-age star cluster BS 90”. In: *The Astrophysical Journal* 664.1 (2007), p. 322.
- [9] Bart J. Van Zeghbroeck. *2.2.5 Temperature dependence of the energy bandgap*. 1996,1997. URL: <https://ecee.colorado.edu/~bart/book/eband5.htm> (visited on 07/12/2019).